This is the accepted manuscript of the article, which has been published in Journal of physical chemistry letters. 2018, 9(9), 2278-2284. http://doi.org/10.1021/acs.jpclett.8b00433

Membrane deformation induces clustering of norovirus bound to glycosphingolipids in a supported cell-membrane mimic

Nagma Parveen[1,], Inga Rimkute[2], Stephan Block[1,‡], Gustaf E. Rydell[3], Daniel Midtvedt[1], Göran Larson[3], Vesa P. Hytönen[4], Vladimir P. Zhdanov[1,5], Anders Lundgren[1,#], Fredrik Höök[1]*

1. Department of Physics, Chalmers University of Technology, Gothenburg, Sweden
2. Department of Clinical Chemistry and Transfusion Medicine, Sahlgrenska Academy, University of Gothenburg, Gothenburg, Sweden
3. Department of Infectious Diseases, Sahlgrenska Academy, University of Gothenburg, Gothenburg, Sweden
4. Faculty of Medicine and Life Sciences and BioMediTech, University of Tampere, Finland and Fimlab Laboratories, Tampere, Finland
5. Boreskov Institute of Catalysis, Russian Academy of Sciences, Novosibirsk, Russia

Present addresses:

*) Laboratory for Photochemistry and Spectroscopy, Department of Chemistry, KU Leuven, Leuven, Belgium

†) Department of Chemistry and Biochemistry, Free University of Berlin, Berlin, Germany

#) Department of Chemistry and Molecular Biology, University of Gothenburg, Gothenburg, Sweden

AUTHOR INFORMATION

Corresponding Author: fredrik.hook@chalmers.se

ABSTRACT

Quartz crystal microbalance with dissipation monitoring and total internal reflection fluorescence microscopy have been used to investigate binding of norovirus-like particles (noroVLPs) to a supported (phospho)lipid bilayer (SLB) containing a few percent of H or B type 1 glycosphingolipid receptors. Although neither of these GSLs spontaneously form domains, noroVLPs were observed to form micron-sized clusters containing typically up to about 30 VLP copies, especially for B type 1 which is a higher-affinity receptor. This novel finding is explained by proposing a model implying that VLP–induced membrane deformation promotes VLP clustering; a hypothesis that was further supported by observing that functionalized gold nanoparticles were able to locally induce SLB deformation. Since similar effects are likely possible also at cellular membranes, our findings are interesting beyond a pure biophysicochemical perspective, as they shed new light on what may happen during receptor-mediated uptake of viruses as well as nano-carriers in drug delivery.

TOC GRAPHICS

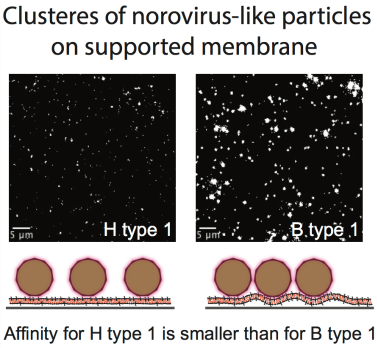

KEYWORDS: virus, glycosphingolipid, supported lipid bilayer, aggregation, lipid domains, binding affinity, membrane deformation

MAIN TEXT

The formation of small protein and lipid clusters or nanoscopic domains in lipid membranes is among the central subjects in current bio-membrane physical chemistry.[1] Another central subject is the interaction of viruses or biologically inspired nanoparticles with lipid membranes.[2-3] Herein, we show how these subareas can merge. Our focus is on the human norovirus, which belongs to the class of non-enveloped RNA viruses. Due to the earlier absence of robust and simple cell culture models of this virus, most of the related *in vitro* studies (see, *e.g.*, Refs. 4-7) have been performed by employing norovirus-like particles (noroVLPs) which are recombinant hollow capsids with a diameter of ~40 nm, each containing about 180 copies of the major capsid protein (VP1). We used such VLPs in combination with a phospholipid bilayer with a few mole percent of H type 1 or B type 1 glycosphingolipids (GSLs), which served as receptors with different affinity to the VP1. The molecular structure of these lipids is the same except for an additional terminal galactose in the oligosaccharide chain of B type 1, a difference sufficient to significantly influence the VLP binding affinity as well as kinetics.[8-9] Fluorescence labelling of hexahistidine-tagged noroVLPs made it possible to combine quartz crystal microbalance with dissipation (QCM–D) monitoring with total internal reflection fluorescence (TIRF) microscopy to investigate VLP binding kinetics and the spatial noroVLP distribution on a laterally mobile supported lipid bilayer (SLB).

In our experiment, the binding affinity of noroVLPs to H type 1 and B type 1 GSLs was compared by using QCM-D to measure the corresponding binding kinetics to SLBs with the GSL concentration ranging from 0.34 to 6.25 mol% (Fig. 1). The initial linear rate of the resonance frequency shift ($d\Delta f/dt$) in QCM–D measurements upon noroVLP binding (see time traces in Fig. S2) displays a non-linear dependence on the GSL concentration in SLB (Fig. 1a) indicating a

transition from reaction- to diffusion-limited kinetics with increasing GSL concentration. For B type 1, this transition occurs at lower GSL concentration and within a ~3 times narrower concentration window compared to H type 1, implying that in the former case the noroVLP achieves a firm attachment involving fewer bonds with GSLs. In other words, the binding affinity (energy of ligand-receptor pair) of noroVLP towards B type 1 is higher, agreeing with previous studies [8-10].

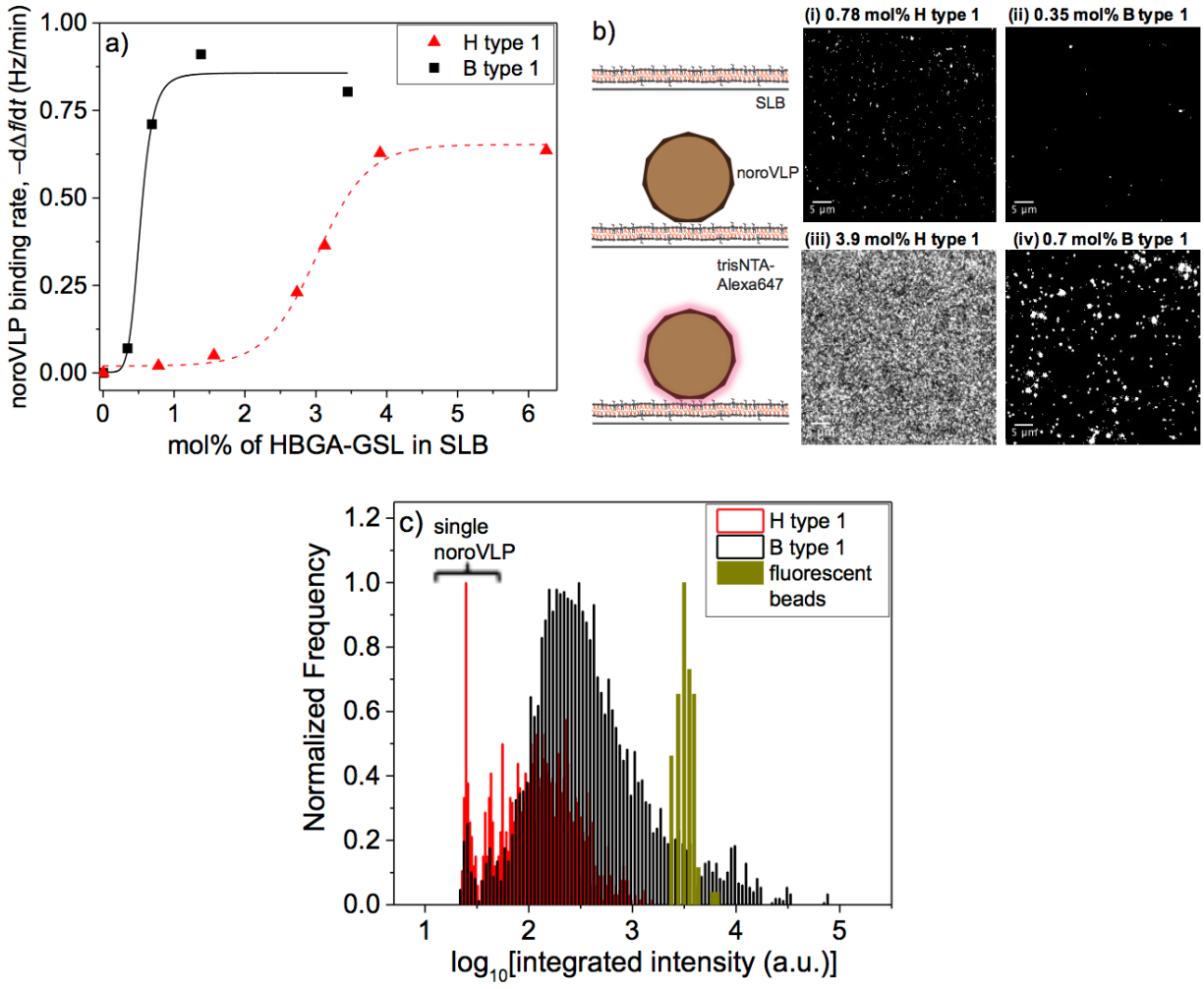

Figure 1. a) Initial rate of binding of noroVLPs obtained from QCM-D measurements, displayed as dΔf/dt versus GSL concentration in SLB. The corresponding QCM–D time traces are shown in Fig. S2. b) A scheme illustrating the post-binding labelling of noroVLPs and TIRF micrographs exhibiting signal from the fluorescently labelled noroVLPs bound to SLB with (i) 0.78 and (iii)

3.9 mol% H type 1, (ii) 0.35 and (iv) 0.7 mol% B type 1 (the intensity contrast of the images is the same except for [iii]). Binding was performed from a 1.1 nM noroVLP suspension with subsequent labelling of bound particles using ~40 nM trisNTA–Alexa647 (details in Sec. S3B). c) Integrated intensity distribution of neutravidin-coated fluorescent beads adhered to a glass surface (as a reference) and noroVLPs on SLBs with 0.78 and 0.7 mol% H type 1 and B type 1, respectively. The images were acquired immediately after post-binding labelling and the intensity distributions were extracted employing the image analysis as described elsewhere[11].

To analyze the spatial distribution of SLB-bound noroVLPs with TIRFM, we implemented a post-binding labelling, *i.e.*, noroVLPs were first bound to the SLB and then labelled with trisNTA–Alexa 647 (see schematic in Fig. 1b and details in Sec. S3B of SI). Due to a nanomolar binding affinity (equilibrium dissociation constant, K_d) of trisNTA towards hexahistidine the conjugation of the fluorescent tags to noroVLPs is essentially irreversible over experimental timescales.[12] The fluorescent signal upon addition of trisNTA–Alexa647 to the SLBs without pre-bound noroVLP was weak (Fig. S5), verifying that the TIRFM micrographs in Fig. 1b [i] and [ii] indeed represent fluorescence staining of noroVLPs, here obtained for SLBs with 0.78 and 0.35 mol% H type 1 and B type 1, respectively. Other than the absolute surface coverage of noroVLP there is hardly any detectable difference in the fluorescence distribution at this low GSL content in the SLB. At increased norovirus coverages obtained at 3.9 and 0.7 mol% of the H type 1 and B type 1, respectively, a difference in the fluorescence distribution is however significant (Fig. 1b [iii] and [iv]). In particular, upon binding to the SLB containing H type 1 the particle fluorescence emission displays a homogeneous distribution, whereas for B type 1, the fluorescent emission appears to originate from discrete objects with a relatively heterogeneous distribution in both their signal intensity and spatial extension (0.5 to 2 μm, *i.e.* beyond the diffraction-limit). Such difference in particle distribution between B type 1 and H type 1 bilayers was observed also at higher GSL concentrations in the SLB (Fig. S8) and within a wide range of noroVLP coverage (Fig. S9).

The integrated fluorescence intensities of discrete particles/objects detected on SLBs with 0.78 mol% H type 1 and 0.7 mol% B type 1 (Fig. 1b [i] and [iv]) were analysed to compare the dependence of the intensity distribution on the receptor type (Fig. 1c). Despite the quite different initial binding rates (Fig. 1a), we chose to compare the particle intensity distribution at a similar total GSL concentration in SLB because the total GSL content appeared to significantly influence the noroVLP coverage. By optimizing the TIRFM measurement conditions we found a comparable window of noroVLP coverage (with a strong enough attachment) on SLBs with ~0.7 mol% of the GSLs, at which single particles and clusters can be discerned. Both intensity distributions in Fig. 1c have an overlapping narrow peak at low intensity, which is attributed to separate single noroVLPs; an interpretation that is supported by the fact that i) noroVLPs are monodisperse (Fig. S1), ii) the labelling distribution is narrow[13] (Sec. S3D), and iii) the intensity distribution width is comparable to that of discrete neutravidin-coated fluorescent beads adhered to a glass surface. Since there were no signs of VLP aggregation in suspension (Sec. S2A), the additional, wider distributions of higher intensities seen in Fig. 1c are attributed to aggregation of noroVLPs after binding. The difference in the wider distribution of higher intensity is likely due to a significantly higher tendency for aggregation of the noroVLPs on the SLB containing the B type 1 compared to the H type 1, which was further supported by similar observations at different noroVLP coverages (Fig. S10). The width of this wider distribution in case of H and B type 1 varies from 1.5 to 3 and 1.5 to 4 in a logarithmic scale, respectively. This means that the aggregates/clusters on H and B type 1 contain roughly from 1 to 30 ($10^{1.5}$) and 1 to 300 ($10^{2.5}$) noroVLPs, respectively. More specifically, the average and FWHM (full width of half maximum) of the cluster intensity distributions on H and B type 1 (Fig. 1c and Fig. S10) indicate that the clusters typically contain from 1 to ~10 and 3 to ~30 noroVLPs, respectively.

To scrutinize the formation kinetics and growth of noroVLP clusters, time-lapse TIRFM movies were acquired during the binding of pre-labelled noroVLPs (fluorescently labelled in suspension, see Sec. S3C) to a SLB with the higher affinity B type 1 receptor (Movie 1). The respective TIRFM micrographs obtained at different time-points display the change of the fluorescent signal upon particle binding together with the appearance of an increasing number of discrete clusters (Fig. 2a). The corresponding ensemble signal intensity has a fast increase (within 12 s) followed by a weak increase over a time period of 22 minutes (black scatter points in Fig. 2b). On closer inspection, the initial intensity rise has a relatively fast component, which is likely to originate from a weak unspecific membrane staining, followed by a slower component attributed to specific noroVLP binding (inset in Fig. 2b). Simultaneously, in addition to the fast intensity rise a slow but substantial increase in the intensity of the signal from the discrete clusters was observed (Fig. 2b). This local signal enhancement proceeded several minutes after noroVLP injection and also after the ensemble signal intensity saturated. These observations imply that after the initial noroVLP binding to B type 1, either newly arrived particles preferentially bind adjacent to the pre-bound particles or the laterally-mobile bound particles prefer to localize at adjacent positions appearing as clusters of bound noroVLPs. The latter type of cluster growth was clearly detected at a few instances (see top panel in Fig. 2a [ii]), but was difficult to quantify statistically due to weak signal per noroVLP and the dye photo-bleaching effect on the signal. Except for few rapidly formed clusters (blue scatter points in Fig. 2b) and stepwise growing clusters (green scatter points in Fig. 2b) most of the clusters show a continuous but saturating growth, as no further increase in signal intensity was detected between 40 minutes to 7 hours after noroVLP addition. A plausible explanation to this observation would be depletion of noroVLP in suspension or B type 1 in the bilayer. However, since further cluster growth was not observed upon replenishing the noroVLP

suspension and a similar trend in the cluster growth was observed on SLBs with a higher (3.45 mol%) B type 1 content (not shown), the observation might, as discussed further below, originate from local depletion of GSLs in SLB induced by local structural alterations of the SLB-noroVLP complexes.

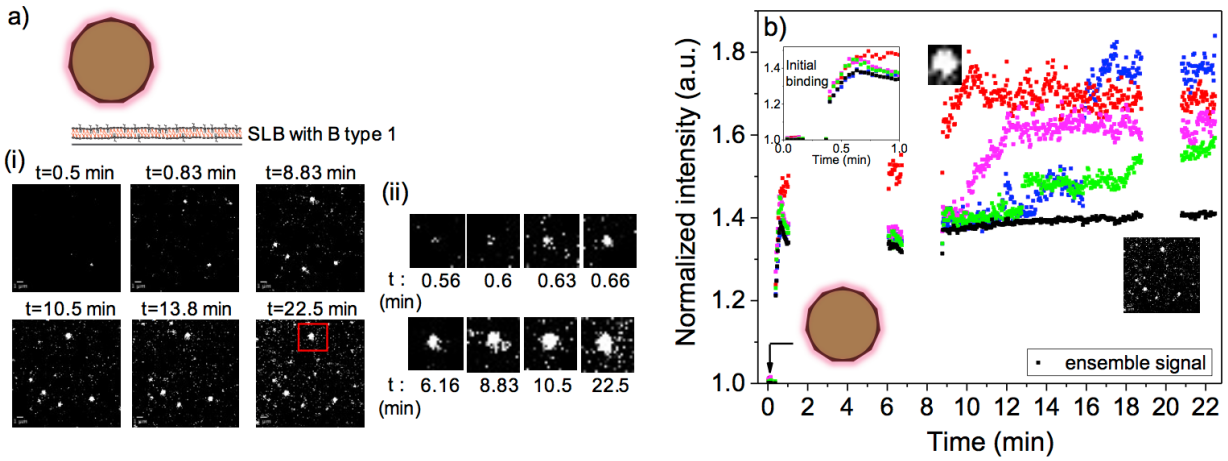

Figure 2. a) Scheme of the binding of fluorescently labelled noroVLPs to B type 1 embedded in the SLB and the corresponding TIRFM micrographs at times as indicated illustrate the change in the fluorescence signal (i) at the ensemble system and (ii) from a growing discrete cluster (in a red square). Size of each TIRFM image in (i) and (ii) is 10 × 10 μm^2 and 3 × 3 μm^2, respectively. b) Change in the normalized average intensity of the ensemble (black scatter points, extracted from 100 × 100 μm^2 TIRFM movie) and from 4 discrete clusters on a SLB with B type 1 during the binding of fluorescent noroVLPs. The binding was done from 0.82 nM fluorescently labelled noroVLPs to a SLB with 0.7 mol% B type 1, see Movie 1. The gaps between the scatter points (between 1-6 min, 6.7-8.7 min, and 18.7-20.8 min) are parts of the measurement when TIRF images were not acquired in order to reduce the photobleaching effect. The data were normalized with respect to the corresponding maximum average intensity.

A plausible explanation to the observed noroVLP cluster formation might be that the relatively high GSL concentration in the membrane induces spontaneous formation of GSL domains prior to noroVLP binding. Such transient submicron liquid-ordered GSL-containing domains were indeed observed[14-15], but only in presence of cholesterol or at very high (50 mol%) sphingomyelin or GSL

content, *i.e.*, conditions very unlike the ones reported herein. It is in this context relevant to stress that non-transient lipid domains tend to fuse together or grow continuously (Ostwald ripening) to eventually form lipid domains of several microns in size.[16-18] However, neither the cluster growth nor the saturation of the growth (Fig. 2b) is consistent with intrinsically formed GSL domains, since this was observed only in response to VLP binding. This interpretation is further supported by experiments in which the SLB-bound noroVLPs were exposed to a fucose-binding lectin that compete with the VLP for binding to the GSLs, a concept that was previously used to scrutinize the nature of multivalent virus interactions[19] by depleting the available receptors. After lectin-addition, the noroVLP clusters became weakly mobile (Movie 2) and multiple instances of cluster division were detected (Fig. S13), observations that both make the existence of glycolipid domains unlikely.

Excluding the possibility of spontaneous GSL-domain formation, we speculate that the clusters observed are inherently related to the SLB–noroVLP interaction. Compared to the protein or lipid domain formation or clustering of small toxins the physics behind virus or VLP clustering in a lipid membrane is expected to be quite different. In particular, due to their small size (~5 nm) proteins are able to directly contact each other near a flat membrane. In contrast, upon binding of viruses or VLPs with a spherical geometry to a flat membrane, the contact region is significantly smaller than the virus or VLP dimension. From geometric consideration, noroVLP (total 180 binding sites) can bind 6 to 10 GSLs under the assumption that the membrane remains flat.[8] In this scenario, even if noroVLPs bind adjacently on the SLB, their contact points will be separated by the diameter of the VLP, *i.e.*, 40 nm, making noroVLP-induced local GSL accumulation very unlikely on a flat SLB. Furthermore, clustering was observed to be significantly more pronounced in the B type 1 case where the ligand-receptor interaction is stronger and thus the formation of a

greater number of bonds between of noroVLP and B type 1 is energetically favorable. Thus, despite the weak energy of the individual interactions, the multivalent interaction could possibly be strong enough to induce local lipid bilayer deformation at the binding sites even in the presence of a solid support underneath the lipid bilayer. To scrutinize this effect, one can first refer to membrane-mediated lateral interaction between attached proteins or colloidal spheres (see Ref. 20 and references therein). The corresponding models are, however, not directly applicable to our case because the noroVLP-SLB interaction occurs via GSLs (1 nm extension of the hydrophilic oligosaccharide unit from the SLB), while in these models proteins/colloids directly interact with a membrane. In addition, these models typically do not take the membrane-support interaction into account.

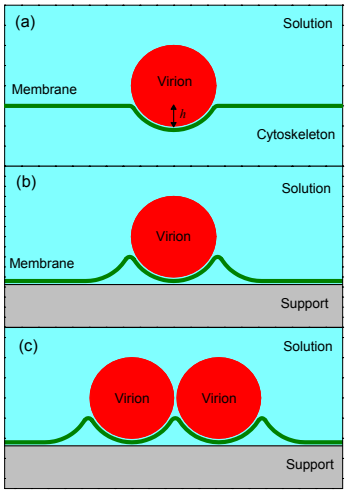

Figure 3. Schemes of lipid-membrane deformation during attachment of a single virus or VLP to (a) a host-cell membrane and (b) supported membrane, and (c) attachment of two viruses or VLPs to a supported membrane. The membrane receptors mediating the attachment are not shown. The interaction of virus/VLPs with the membrane occurring via receptors is considered to be appreciable so that it results in the local rupture of the membrane-support bonds and membrane bending. Note that after the addition of the second particle [(c) vs. (b)] the membrane-particle contact area calculated per particle does not change while the area of the bended membrane and the area of the region where the membrane-support bonds are broken (both areas are considered to

be calculated per particle) become smaller. The membrane-particle contacts are energetically favourable, their relative role becomes higher if two particles are located nearby, and accordingly such particle arrangements are preferable.

A more relevant class of models for our system are those focusing on virus entry into cells by endocytosis,[21-22] as schematically illustrated in Fig.3. In such models, the interaction energy of a virus with the host cell is typically represented as $E = E_r + E_b + E_c$, where E_r, E_b, E_c are the energy terms corresponding to the attractive interaction with membrane receptors, membrane bending, and deformation of cytoskeleton or, more specifically, of actin filaments, respectively (see corresponding expressions in Sec. S4). During the initial phase of virus entry (at engulfment depth $h <$ virus radius, see Fig 3a) E_c is negligible[22] and the process is often energetically favorable provided $|E_r| > E_b$. In our case (Fig. 3b), by analogy, the interaction energy can be rewritten as, $E = E_r + E_b + E_s$, where E_s is the energy needed to rupture membrane-support bonds (details in Sec. S4). The rupture of the membrane-support bonds is energetically favorable provided that $|E_r| > E_b + E_s$. If the rupture of the membrane-support bonds takes place, the membrane bending near a bound virus/VLP may be appreciable and cause a local membrane deformation. In this case, the adjacent location of virus/VLP (Fig. 3c) becomes energetically favorable because it allows the particle to gain more contact area, *i.e.*, more VLP-GSL bonds can be formed, as well as reduce both the membrane bending energy and the energy needed to rupture the membrane-support bonds. As a result, particles will experience a locally attractive membrane-mediated lateral interaction. Each energy term in the latter energy expression is considerably greater than k_BT and accordingly the attractive membrane-mediated particle-particle interaction can be much larger as well. As detailed in Supporting Information, the VLP-GSL contact has for B type 1 a relatively high affinity (on the scale of 7 k_BT) suggesting that membrane deformation would be energetically favorable.

As a consequence of such a structural deformation of the SLB, the free diffusion of available GSLs may be hindered and result a local depletion of receptors and thereby a saturating growth of the clusters. Importantly, these arguments are qualitatively applicable not only to viruses/VLPs attachment to a SLB but also to attachment of viruses to the cell membranes and their aggregation prior to membrane invagination (the latter was scrutinized in Refs. 20 and 23), because the structures of the expressions for the interaction energies are similar.

To further support the feasibility of such local SLB deformation upon particle attachment, we used QCM-D to track irreversible binding of synthetic model noroVLPs or, more specifically, of gold-PEG core-shell nanoparticles with a hydrodynamic diameter of ~40 nm displaying 50-60 biotin ligands at their periphery[24] to both a biotinylated SLB (mobile) and thiol-PEG-biotin (immobile) functionalized surface via a linker layer of streptavidin (Fig. 4). Even at the same streptavidin coverage, the corresponding saturated particle coverage was lower on the SLB than on the thiol–PEG functionalized surface. This is attributed to the fact that mobile biotins in the SLB "recruit" mobile streptavidin at adjacent positions, thereby increasing the number of bound streptavidin per particle while lowering the number of available streptavidin on the surface. On a thiol–PEG surface, however, the conjugated streptavidin is immobile, thus the number of available streptavidin within the nanoparticle contact area is limited and, accordingly, surface-bound streptavidin cannot be depleted due to multivalent nanoparticle–streptavidin interaction. Further, upon subsequent injection of streptavidin to the gold particles bound on the thiol–PEG surface, the observed response shows that multiple biotin binding sites on bound nanoparticles are not yet engaged in bonds and thus still available. In contrast, SLB-bound gold nanoparticles barely showed any additional streptavidin binding (Fig. 4b), indicating that a majority of the biotins on the nanoparticles were already engaged in binding with streptavidin on the SLB. To explain this, we

argue that a rigid thiol-PEG surface is unable to deform, while a SLB is flexible enough to partially wrap the bound nanoparticles, as schematically illustrated in Fig. 4a, thereby lowering the number of available streptavidin binding sites (*i.e.*, biotins). This interpretation is further supported by light scattering and confocal imaging measurements, demonstrating a drastic reduction in mobility for gold nanoparticles engaging multiple ligand-receptor pairs and membrane restructuring in the contact region, respectively (Sec. S3K, Supporting Information).

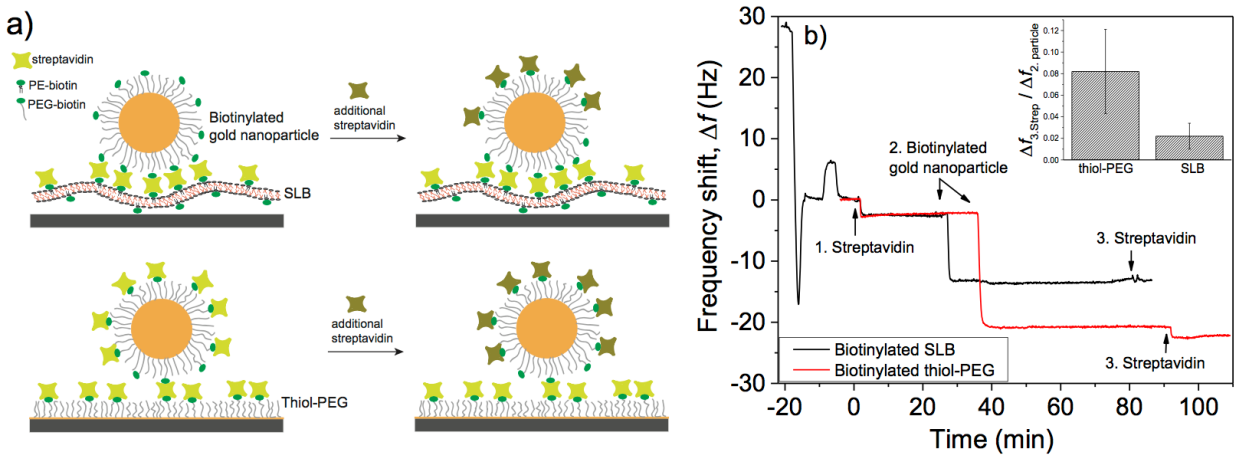

Figure 4. a) Scheme of a sandwich binding assay on a mobile SLB and an immobile thiol–PEG functionalized surface using biotinylated gold nanoparticles 40 nm in diameter. b) Time-trace of resonance frequency change (3rd overtone) in QCM–D upon subsequent binding of streptavidin, biotinylated gold nanoparticles, and streptavidin to a biotinylated SLB and a surface functionalized with thiol–PEG-biotin. Formation of a SLB on a silica-coated QCM–D sensor is characterized with a two-phase change in the frequency upon injection of biotinylated lipid vesicles. The gold coated QCM–D sensor was functionalized with thiol–PEG-biotin prior to mounting it in the QCM–D instrument. To achieve the same streptavidin coverage on both surfaces, the biotin content in the SLB and on the thiol–PEG functionalized surface was adjusted accordingly. The inset shows the ratio of the final frequency shift upon injection of streptavidin (third step) and the corresponding shift for gold nanoparticle binding (second step). Error bars represent the statistical deviation.

In conclusion, we show in this work that the binding kinetics of noroVLPs differed significantly between two GSLs, with higher affinity for B type 1 compared to H type 1 receptors (Fig. 1). However, somewhat unexpectedly, despite any indications of GSL aggregation in the SLBs, also the tendency to form small-scale noroVLP aggregates was observed, in particular on SLBs containing the higher-affinity receptor B type 1. Our results also suggest that SLBs can indeed be locally deformed upon attachment of nanoparticles and qualitatively explains the mechanism of noroVLP cluster formation on SLBs containing a relatively high affinity GSL receptor in line with the model suggested above to explain VLP clustering. In the related context of protein clustering on cell membranes, this phenomenon has long been associated with lipid sorting in membranes[25], trans-signalling between lipid layers[26], and their endocytosis[20]. Thus membrane-deformation induced virus clustering on cell membranes might also function as signaling intermediates or low energy transition states between bound and internalized state as described by recent theoretical studies.[23] Another related remark is that the induction of membrane invaginations on giant uni-lamellar vesicles (GUVs) was previously studied with noroVLPs of the Dijon strain[27]. Similar membrane invaginations were observed also for the polyomavirus SV40, and have been suggested to correspond to endocytosis intermediates.[28] Even though the noroVLP tubulation study[27] was not quantitative, a tendency towards more efficient invagination on GUVs with B type 1 than H type 1 was observed, which is in agreement with our results of preferential noroVLP clustering on SLB with B type 1. Further, the interaction between SV40 and its GSL receptor GM1 has been thoroughly characterized in terms of affinity, multivalency and diffusion of the virus-receptor complex on the cell surface as well as endocytosis.[19, 28-30] In terms of the equilibrium dissociation constant, K_d, the corresponding affinity of SV40[19, 31] appears to be in between that of H type 1[32] and B type 1.[32] Our already mentioned estimates show that the physically reasonable virus-receptor

interaction on the scale of 7 k_BT is sufficient for rupture of the membrane-support bonds and VLP clustering, suggesting that a similar mechanism to that observed in this work is plausible also in the case of SV40. Taken together, earlier observations and our results indicate that the hypothesis of virus/VLPs clustering is conceptually important in the context of viral endocytosis, suggesting that future experiments should focus on imaging with improved temporal and lateral resolution, using GSLs and virus strains with significant different affinities and labeling strategies capable of resolving structural change at the molecular scale. Finally, our results are also of interest from the perspectives of the use of biologically-inspired nanoscale carriers for intracellular delivery of e.g. RNA (this approach is considered to have great potential in therapeutics[3]), because the interaction of such carriers with the host-cell membrane is similar to that of viruses.

ASSOCIATED CONTENT

Supplementary Information. The Supplementary information contains additional materials and methods, preparation details, and supporting QCM-D and TIRFM experiments, the expression of the energy terms specifying the theoretical model suggested as well as videos representing the micrographs in Figs. 1 and 2.

AUTHOR INFORMATION

Author Contributions

N.P. did the QCM-D measurements and N.P. and I.R. performed TIRFM experiments of noroVLPs, A.L. provided the experimental data of gold nanoparticles,, N.P. and S.B. analyzed the data, V.P.Z. developed the theory. N.P., V.P.Z., G.L., V.H. and F.H. conceived the project and wrote the article together with A.L., S.B., and G.E.R. All coauthors gave permission to write the article.

Funding Sources

The research leading to these results received funding from the Swedish Research Council under grants 2013-7421 (A.L.) and 2014-5557 (A.L., V.P.Z., F.H.), the Swedish Foundation for Strategic Research under grant no. RMA11-0104 (A.L., F.H.).

Notes

The authors have no competing financial interests.

REFRENCES

1. Sezgin, E.; Levental, I.; Mayor, S.; Eggeling, C. The mystery of membrane organization: composition, regulation and roles of lipid rafts. *Nat. Rev. Mol. Cell Biol.* **2017,** *18* (6), 361-374.

2. Cossart, P.; Helenius, A. Endocytosis of Viruses and Bacteria. *Cold Spring Harb. Perspect. Biol.* **2014,** *6* (8), 28.

3. Dowdy, S. F. Overcoming cellular barriers for RNA therapeutics. *Nat. Biotechnol.* **2017,** *35* (3), 222-229.

4. Ettayebi, K.; Crawford, S. E.; Murakami, K.; Broughman, J. R.; Karandikar, U.; Tenge, V. R.; Neill, F. H.; Blutt, S. E.; Zeng, X. L.; Qu, L.; Kou, B.; Opekun, A. R.; Burrin, D.; Graham, D. Y.; Ramani, S.; Atmar, R. L.; Estes, M. K. Replication of human noroviruses in stem cell-derived human enteroids. *Science* **2016,** *353* (6306), 1387-1393.

5. Hutson, A. M.; Atmar, R. L.; Marcus, D. M.; Estes, M. K. Norwalk virus-like particle hemagglutination by binding to H histo-blood group antigens. *J. Virol.* **2003,** *77* (1), 405-415.

6. Marionneau, S.; Ruvoen, N.; Le Moullac-Vaidye, B.; Clement, M.; Cailleau-Thomas, A.; Ruiz-Palacois, G.; Huang, P. W.; Jiang, X.; Le Pendu, J. Norwalk virus binds to histo-blood group antigens present on gastroduodenal epithelial cells of secretor individuals. *Gastroenterology* **2002,** *122* (7), 1967-1977.

7. Nilsson, J.; Rydell, G. E.; Le Pendu, J.; Larson, G. Norwalk virus-like particles bind specifically to A, H and difucosylated Lewis but not to B histo-blood group active glycosphingolipids. *Glycoconj. J.* **2009,** *26* (9), 1171-1180.

8. Bally, M.; Gunnarsson, A.; Svensson, L.; Larson, G.; Zhdanov, V. P.; Hook, F. Interaction of single viruslike particles with vesicles containing glycosphingolipids. *Phys. Rev. Lett.* **2011,** *107* (18), 188103.

9. Rydell, G. E.; Dahlin, A. B.; Hook, F.; Larson, G. QCM-D studies of human norovirus VLPs binding to glycosphingolipids in supported lipid bilayers reveal strain-specific characteristics. *Glycobiology* **2009,** *19* (11), 1176-1184.

10. Nasir, W.; Frank, M.; Kunze, A.; Bally, M.; Parra, F.; Nyholm, P.-G.; Höök, F.; Larson, G. Histo-blood group antigen presentation is critical for binding of norovirus VLP to glycosphingolipids in model membranes. *ACS Chem. Biol.* **2017,** *12* (5), 1288-1296.

11. Block, S.; Fast, B. J.; Lundgren, A.; Zhdanov, V. P.; Hook, F. Two-dimensional flow nanometry of biological nanoparticles for accurate determination of their size and emission intensity. *Nat. Commun.* **2016,** *7*, 8.

12. Lata, S.; Gavutis, M.; Tampe, R.; Piehler, J. Specific and stable fluorescence labeling of histidine-tagged proteins for dissecting multi-protein complex formation. *J. Am. Chem. Soc.* **2006,** *128* (7), 2365-2372.

13. Koho, T.; Ihalainen, T. O.; Stark, M.; Uusi-Kerttula, H.; Wieneke, R.; Rahikainen, R.; Blazevic, V.; Marjomaki, V.; Tampe, R.; Kulomaa, M. S.; Hytonen, V. P. His-tagged norovirus-like particles: A versatile platform for cellular delivery and surface display. *Eur. J. Pharm. Biopharm.* **2015,** *96*, 22-31.

14. de Wit, G.; Danial, J. S. H.; Kukura, P.; Wallace, M. I. Dynamic label-free imaging of lipid nanodomains. *Proc. Natl. Acad. Sci. U. S. A.* **2015,** *112* (40), 12299-12303.

15. Raghupathy, R.; Anilkumar, A. A.; Polley, A.; Singh, P. P.; Yadav, M.; Johnson, C.; Suryawanshi, S.; Saikam, V.; Sawant, S. D.; Panda, A.; Guo, Z.; Vishwakarma, R. A.; Rao, M.; Mayor, S. Transbilayer lipid interactions mediate nanoclustering of lipid-anchored proteins. *Cell* **2015,** *161* (3), 581-594.

16. Harder, T.; Scheiffele, P.; Verkade, P.; Simons, K. Lipid domain structure of the plasma membrane revealed by patching of membrane components. *J. Cell Biol*. **1998,** *141* (4), 929-942.

17. Romer, W.; Berland, L.; Chambon, V.; Gaus, K.; Windschiegl, B.; Tenza, D.; Aly, M. R. E.; Fraisier, V.; Florent, J. C.; Perrais, D.; Lamaze, C.; Raposo, G.; Steinem, C.; Sens, P.; Bassereau, P.; Johannes, L. Shiga toxin induces tubular membrane invaginations for its uptake into cells. *Nature* **2007,** *450* (7170), 670-U3.

18. Windschiegl, B.; Orth, A.; Romer, W.; Berland, L.; Stechmann, B.; Bassereau, P.; Johannes, L.; Steinem, C. Lipid reorganization induced by shiga toxin clustering on planar membranes. *PLoS One* **2009,** *4* (7), 11.

19. Parveen, N.; Block, S.; Zhdanov, V. P.; Rydel, G. E.; Hook, F. Detachment of membrane bound virions by competitive ligand binding induced receptor depletion. *Langmuir* **2017,** *33* (16), 4049-4056.

20. Reynwar, B. J.; Illya, G.; Harmandaris, V. A.; Muller, M. M.; Kremer, K.; Deserno, M. Aggregation and vesiculation of membrane proteins by curvature-mediated interactions. *Nature* **2007,** *447* (7143), 461-464.

21. Vacha, R.; Martinez-Veracoechea, F. J.; Frenkel, D. Receptor-mediated endocytosis of nanoparticles of various shapes. *Nano Lett*. **2011,** *11* (12), 5391-5395.

22. Zhdanov, V. P. Kinetics of virus entry by endocytosis. *Phys. Rev. E* **2015,** *91* (4), 7.

23. Saric, A.; Cacciuto, A. Mechanism of membrane tube formation induced by adhesive nanocomponents. *Phys. Rev. Lett*. **2012,** *109* (18), 5.

24. Lundgren, A.; Agnarsson, B.; Zirbs, R.; Zhdanov, V. P.; Reimhult, E.; Hook, F. Nonspecific colloidal-type interaction explains size-dependent specific binding of membrane-targeted nanoparticles. *ACS Nano* **2016,** *10* (11), 9974-9982.

25. Sorre, B.; Callan-Jones, A.; Manneville, J. B.; Nassoy, P.; Joanny, J. F.; Prost, J.; Goud, B.; Bassereau, P. Curvature-driven lipid sorting needs proximity to a demixing point and is aided by proteins. *Proc. Natl. Acad. Sci. U. S. A.* **2009,** *106* (14), 5622-5626.

26. Lingwood, D.; Simons, K. Lipid rafts as a membrane-organizing principle. *Science* **2010,** *327* (5961), 46-50.

27. Rydell, G. E.; Svensson, L.; Larson, G.; Johannes, L.; Romer, W. Human GII.4 norovirus VLP induces membrane invaginations on giant unilamellar vesicles containing secretor gene dependent alpha 1,2-fucosylated glycosphingolipids. *Biochim. Biophys. Acta-Biomembr.* **2013,** *1828* (8), 1840-1845.

28. Ewers, H.; Romer, W.; Smith, A. E.; Bacia, K.; Dmitrieff, S.; Chai, W. G.; Mancini, R.; Kartenbeck, J.; Chambon, V.; Berland, L.; Oppenheim, A.; Schwarzmann, G.; Feizi, T.; Schwille, P.; Sens, P.; Helenius, A.; Johannes, L. GM1 structure determines SV40-induced membrane invagination and infection. *Nat. Cell Biol.* **2010,** *12* (1), 11-U36.

29. Kukura, P.; Ewers, H.; Muller, C.; Renn, A.; Helenius, A.; Sandoghdar, V. High-speed nanoscopic tracking of the position and orientation of a single virus. *Nat. Methods* **2009,** *6* (12), 923-927.

30. Szklarczyk, O. M.; Gonzalez-Segredo, N.; Kukura, P.; Oppenheim, A.; Choquet, D.; Sandoghdar, V.; Helenius, A.; Sbalzarini, I. F.; Ewers, H. Receptor concentration and diffusivity control multivalent binding of SV40 to membrane bilayers. *PLoS Comput. Biol.* **2013,** *9* (11), e1003310.

31. Neu, U.; Woellner, K.; Gauglitz, G.; Stehle, T. Structural basis of GM1 ganglioside recognition by simian virus 40. *Proc. Natl. Acad. Sci. U.S.A.* **2008,** *105* (13), 5219-5224.

32. Mallagaray, A.; Lockhauserbäumer, J.; Hansman, G.; Uetrecht, C.; Peters, T. Attachment of norovirus to histo blood group antigens: a cooperative multistep process. *Angew. Chem. Int. Ed.* **2015,** *54* (41), 12014-12019.